Journal of Power Sources 180 (2008) 875–879

Contents lists available at ScienceDirect

Journal of Power Sources

journal homepage: www.elsevier.com/locate/jpowsour

Short communication

MW-assisted synthesis of $LiFePO_4$ for high power applications

Sabina Beninati, Libero Damen, Marina Mastragostino*

University of Bologna, Department of Metal Science, Electrochemistry and Chemical Techniques, Via San Donato 15, 40127 Bologna, Italy

ARTICLE INFO

Article history:
Received 24 January 2008
Received in revised form 21 February 2008
Accepted 24 February 2008
Available online 29 February 2008

Keywords:
Lithium iron phosphate
Microwave synthesis
Cathode materials
Batteries for HEV

ABSTRACT

$LiFePO_4$/C was prepared by solid-state reaction from Li_3PO_4, $Fe_3(PO_4)_2{\cdot}8H_2O$, carbon and glucose in a few minutes in a scientific MW (microwave) oven with temperature and power control. The material was characterized by X-ray diffraction, scanning electron microscopy and by TGA analysis to evaluate carbon content. The electrochemical characterization as positive electrode in EC (ethylene carbonate)–DMC (dimethylcarbonate) 1 M $LiPF_6$ was performed by galvanostatic charge–discharge cycles at C/10 to evaluate specific capacity and by sequences of 10 s discharge–charge pulses, at different high C-rates (5–45C) to evaluate pulse-specific power in simulate operative conditions for full-HEV application. The maximum pulse-specific power and, particularly, pulse efficiency values are quite high and make MW synthesis a very promising route for mass production of $LiFePO_4$/C for full-HEV batteries at low energy costs.

1. Introduction

Since the work of Goodenough and co-workers [1], the $LiFePO_4$ has been recognized as a promising positive electrode material for lithium rechargeable batteries because of its low cost, environmental compatibility and theoretical specific capacity of 170 mAh g^{-1}. Today it is under investigation for lithium-ion battery application in second generation full hybrid electric vehicles (HEVs) [2].

Several approaches have been pursued to achieve the theoretical capacity at room temperature (RT) including decreasing particle size, particle coating with carbon [3] or co-synthesis of the compound with carbon [4,5], addition of metals [6] or Fe_2P [7], and selective $LiFePO_4$ doping with supervalent cations to enhance lattice electronic conductivity [8]. Several kinds of synthesis have also been employed, including solid-state reaction, sol–gel, mechanochemical, hydrothermal, coprecipitation in aqueous medium, and more recently microwave (MW) synthesis [9–17]. Unlike the rapid MW-assisted syntheses, all the other methods require a final heating step of several hours at high temperatures in inert or reductive atmosphere (12–15 h at 500–700 °C under Ar or Ar/H_2) to yield $LiFePO_4$ in the crystalline phase, with the exception of a long-duty time mechanochemical method involving higher temperatures over shorter time [11]. The first MW synthesis of $LiFePO_4$ was carried out by Higuchi et al. [13] in a MW domestic oven (2.45 GHz) in Ar atmosphere for a few minutes starting from Li_2CO_3, $NH_4H_2PO_4$ and iron (II) acetate or lactate. Park et al. [14] used MW heating as an alternative to a furnace to crystallize $LiFePO_4$, given that it was hard to prepare the pure iron (II) compound in a furnace, and they added activated carbon to the $LiFePO_4$. Carbon, which is a MW susceptor, provided rapid heating and its partial oxidation to CO_2 produced a reductive atmosphere which preserved the iron (II) in its oxidation state. More recently, Song et al. [15] irradiated in a domestic MW oven a mixture of Li_3PO_4, $Fe_3(PO_4)_2{\cdot}8H_2O$ and carbon, previously ground in a high energy ball-mill, to obtain fine particles of $LiFePO_4$. Wang et al. [16] prepared $LiFePO_4$ by MW irradiation of $NH_4H_2PO_4$, CH_3COOLi and $FeC_2O_4{\cdot}2H_2O$ mixed with different amounts of citric acid in a self-assembly carbon seal reactor. Li et al. [17] synthesized $LiFePO_4$ from $NH_4FePO_4{\cdot}H_2O$, Li_3PO_4 and sugar mixed by ball milling for 24 h and pressed into pellets which were put inside an alumina crucible filled with carbon and irradiated in a MW domestic oven for different time from 5 to 20 min.

MW synthesis of $LiFePO_4$, which has the great advantage of short synthesis time in air instead of Ar or Ar–H_2 atmosphere as in lengthy furnace firing processes, is a promising approach to mass $LiFePO_4$ production at low-energy cost for HEV application. Given that there has been no investigation of MW synthesized $LiFePO_4$ for HEV application, we performed several MW syntheses of this material in a scientific MW oven starting from a solid mixture of Li_3PO_4, $Fe_3(PO_4)_2{\cdot}8H_2O$, carbon and glucose. After structural and morphological characterization, we electrochemically investigated

* Corresponding author. Tel.: +39 051 2099798; fax: +39 051 2099365.
E-mail address: marina.mastragostino@unibo.it (M. Mastragostino).

0378-7753/$ – see front matter © 2008 Elsevier B.V. All rights reserved.
doi:10.1016/j.jpowsour.2008.02.066

the synthesized materials by pulse tests at high C-rate for full-HEV application. The results are reported and discussed.

2. Experimental

The scientific MW oven (2.45 GHz) was a single-mode CEM Discover connected to an air compressor system that automatically provided cooling and assisted the MW power tuning in order to not overcome the maximum set temperature (T_{max}). This apparatus, described in details elsewhere [18], operates in continuous power generation from 0 to 300 W and the maximum programmable T_{max} is 300 °C, measured at the bottom of the sample quartz vessel of 10 ml by an internal infrared sensor located below the MW cavity. An external pyrometer (Impac-Mikron infrared pyrometer) was also used to monitor the surface temperature of the sample upon the synthesis.

The MW syntheses of $LiFePO_4$ were carried out by irradiating 0.7 g of sample containing 88.0 wt% of $Fe_3(PO_4)_2{\cdot}8H_2O$ (home prepared) and Li_3PO_4 (Aldrich) in the stoichiometric ratio, 3.4 wt% carbon (SuperP Erachem) and 8.6 wt% glucose (D-(+)-Glucose ACS reagents, Sigma–Aldrich), previously ground in an agate jar by ball milling at 250 rpm for 30 min, and the MW power and T_{max} were set at 300 W and 300 °C, respectively. The precursor $Fe_3(PO_4)_2{\cdot}8H_2O$ was prepared in de-ionized water from $FeSO_4{\cdot}7H_2O$ (Aldrich) and *ortho*-phosphoric acid (Fluka, ≥99%) in the molar ratio 1:1 at pH 11.0 and dried at room temperature to avoid elimination of H_2O molecules from the crystalline structure.

X-ray diffraction (XRD) analysis of the powders was performed with a Philips PW1710 diffractometer, a Cu Kα (λ = 1.5406 Å) radiation source and Ni filter, with continuous acquisition in 10–80° 2θ range, 0.05° 2θ s^{-1} scan rate; infrared spectrum was collected by a FT-IR Nicolet 380 spectrometer with 32 scans in the range 4000–400 cm^{-1} and 4 cm^{-1} resolution; the scanning electron micrographs (SEM) were acquired with a Zeiss EVO 50 apparatus; the nitrogen adsorption porosimetry measurements were carried out on the powders, dried for 2 h at 80 °C before testing, by Micromeritics ASAP 2020 system. The thermogravimetric analysis (TGA) was carried out by Mettler Toledo TGA/SDTA A851 from room temperature to 700 °C with a heating rate of 5 °C min^{-1} in O_2 flux.

Electrochemical characterizations were performed on electrodes prepared as follows: a mixture of $LiFePO_4$/C and carbon Super P in appropriate ratio was ground by ball milling at 500 rpm for 1 h in agate jar with water addition (10 ml), dried at 120 °C under vacuum overnight, and added to a poly(vinylidene fluoride) (PVdF, Fluka) solution in *N*-methyl-2-pyrrolidone (Fluka); the slurry was spread on aluminium current collector (10 μm thickness) by doctor blade technique and then dried at 100 °C for 12 h under dynamic vacuum. The electrode composition was 78 wt% $LiFePO_4$/C, 14 wt% carbon conducting additive and 8 wt% PVdF binder, the electrode area ca. 0.6 cm^2 and the loading of the active material ca. 3–4 mg cm^{-2}. The electrochemical cells were "T-type" with Li in excess as the counter electrode and Li as reference electrode; a dried and degassed glass separator (Whatman GF/D 400 μm thick) was used after soaking in the same electrolyte used in the electrochemical cell, ethylene carbonate (EC):dimethylcarbonate (DMC) 2:1–1 M $LiPF_6$ (Merck LP31). The cell assembling and sealing were performed in argon atmosphere MBraun Labmaster 130 dry box (H_2O and O_2 < 1 ppm) and the cells were tested from RT to 60 °C by deep galvanostatic charge–discharge cycles at C/10 for the evaluation of the reversible specific capacity, and at RT by sequences (10 or 100) of 10 s discharge and 10 s charge pulses at different high C-rates (5–45C) with 5 min rest between each pulse, for evaluation of the pulse-specific powers in simulated operative conditions for full-HEV application. The HEV pulse tests were performed after discharging the cell to 50% DOD at C/10. All the electrochemical tests were carried out by PerkinElmer VMP multichannel potentiostat.

3. Results and discussion

3.1. MW synthesis and structural—morphological characterization

Starting from solid mixtures of Li_3PO_4–$Fe_3(PO_4)_2{\cdot}8H_2O$–carbon–glucose of same composition, we performed several MW syntheses in air by setting MW power and T_{max} at the maximum values for the scientific MW oven (300 W and 300 °C) so as to minimize synthesis time. The carbon in the mixture absorbs MW radiation, and the glucose was added to provide the carbon coating of the final product, which in turn should even inhibit crystal growth, as reported in Ref. [19]. During all the syntheses, temperature was monitored by the two sensors, the internal pyrometer which tunes the MW power and triggers the cooling system, and the external which monitors the temperature of the sample surface. Fig. 1 shows the MW power and temperature profiles, which are representative for all the syntheses in these conditions. During the first 300 s, the oven provides MW irradiation at the set value of 300 W, at the beginning the temperature monitored by the two sensors slightly increases to 120 °C; thereafter the two temperatures differ, the external increasing and the internal remaining almost constant until its abrupt increase (also recorded by external sensor) to the T_{max} value of 300 °C. The feedback system then tunes the MW radiation power to ca.10 W and the air-compressor automatically provides cooling to maintain the temperature at 300 °C. All syntheses were stopped after the abrupt temperature increase, i.e. after MW radiation of 4.5–6.5 min (after 350 s for the synthesis in Fig. 1).

All the XRD analyses performed on synthesized materials displayed the same diffraction pattern and, as shown in Fig. 2, the peaks correspond to those of the $LiFePO_4$ (the standard $LiFePO_4$ XRD is also reported in the figure), thus demonstrating the effectiveness of MW syntheses in the production of a pure $LiFePO_4$ crystalline phase in a few minutes. The crystallite size was evaluated from

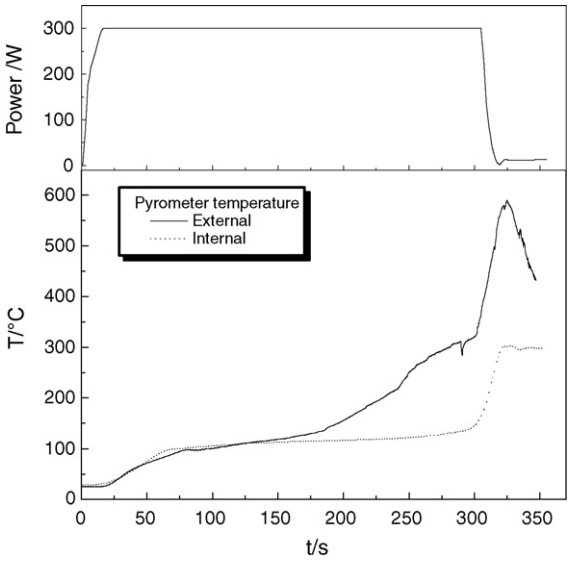

Fig. 1. MW power and temperature profiles detected by the internal (dot line) and the external (continuous line) pyrometer.

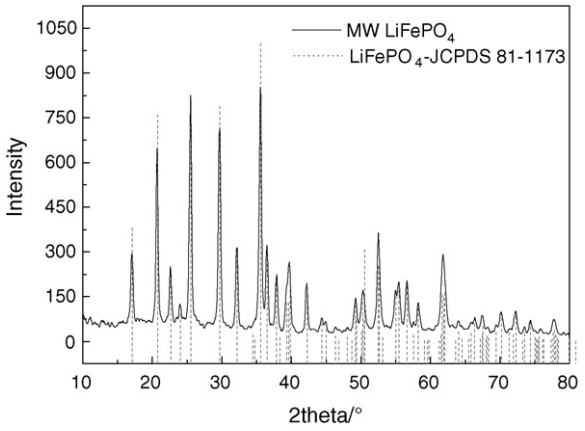

Fig. 2. X-ray diffraction pattern of the MW synthesized and the standard $LiFePO_4$.

the 200 peaks by Scherrer's equation and the values were in the range of 20–37 nm. The crystallites are significantly smaller than those of $LiFePO_4$ prepared by solid-state synthesis with annealing at 600 °C for 18 h (125 nm) [9] or by mechanochemical synthesis followed by heat treatment in the range 550–800 °C for a shorter time (77–520 nm) [11].

Although the crystallites compare well to those of other MW synthesized $LiFePO_4$ (24, 35 58 and 36 nm for MW radiation time of 5, 10, 15 and 20 min) [17], we were unable to control in our reported range their size by synthesis time. This because the effective $LiFePO_4$ synthesis mainly occurs in less than 1 min during the abrupt increase in temperature. This is demonstrated in Fig. 3, which displays the XRD patterns of samples A and B that were the products of the MW syntheses that were stopped before this rapid increase, i.e. 150 s (sample A) and 275 s (sample B) from the beginning of MW radiation.

Fig. 3 also shows for comparison the XRD profiles of the precursors Li_3PO_4 and $Fe_3(PO_4)_2{\cdot}8H_2O$ and clearly evinces that only the precursors are present in sample A and that a small amount of $LiFePO_4$ was produced in sample B. Furthermore, given that during MW heating of carbon alone (result not displayed here) the temperature quickly increases to 600–1000 °C the slow initial increase during the MW syntheses of $LiFePO_4$ is related to a *restraining effect* of the precursors on the MW carbon heating: the precursors, which do not absorb the MW radiation, are heated by the carbon, and heat is also involved in the evaporation of the crystallization water of the $Fe_3(PO_4)_2{\cdot}8H_2O$. Once the water has completely evaporated, the internal sensor detects the temperature increase after the external sensor does. This is presumably due to the different location of the sensors, i.e. the external is directly on the powder and the internal at the bottom of the sample that is in a quartz vessel which is MW transparent and heated by conduction. However, given that it is toward the end of the process that the MW radiation provides the large amount of $LiFePO_4$, and given the delay of the internal sensor, we can state that the final product experienced temperatures higher than 300 °C for no more than 1 min, reaching a maximum 600–700 °C for a few seconds, i.e. a time which is too short for feasible control of crystallite size.

FT-IR analysis was performed on the MW synthesized material. Fig. 4, which displays the transmittance spectrum, shows that all the bands are characteristic of $LiFePO_4$ [20] to the exclusion of a no-recognized, low-intensity band at 1400 cm^{-1}, which we think is due to a negligible impurity.

Given that we expected to synthesize carbon-coated materials the amount of carbon was evaluated by TGA analysis as in Ref. [21].

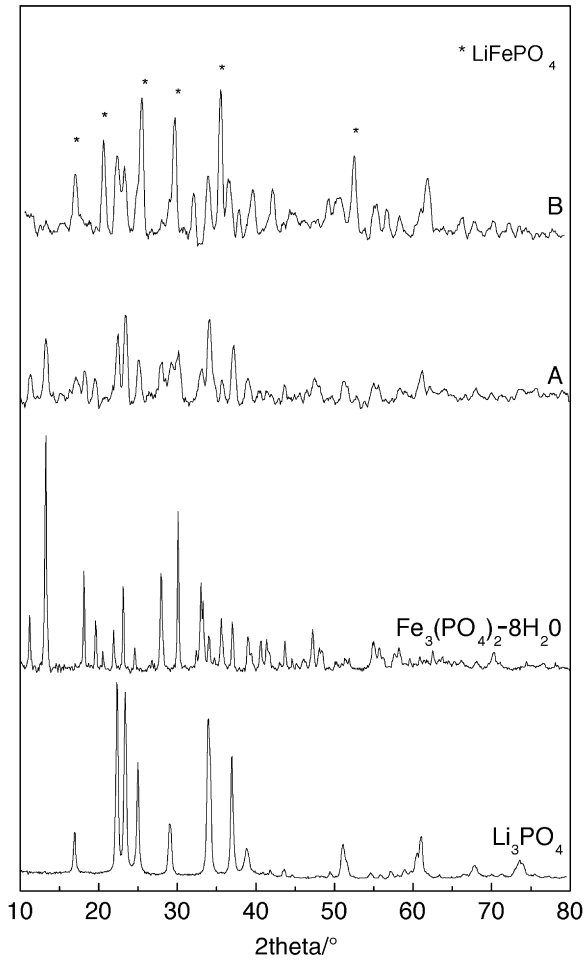

Fig. 3. X-ray diffraction patterns of the sample A, sample B, and of the precursors $Fe_3(PO_4)_2{\cdot}8H_2O$ and Li_3PO_4.

Fig. 5 shows an example of TGA analysis: the sample is heated in an O_2 flux up to 700 °C and the weight loss is 0.9%. Given that the $LiFePO_4$ is completely oxidized to $Li_3Fe_2(PO_4)_3$ and Fe_2O_3 at this temperature [22], the weight should increase by 5.1%, and a decrease of 0.9% indicates a carbon content in the $LiFePO_4$/C sample of 6 wt%. Samples of different MW syntheses displayed C content in the 3–6 wt% range.

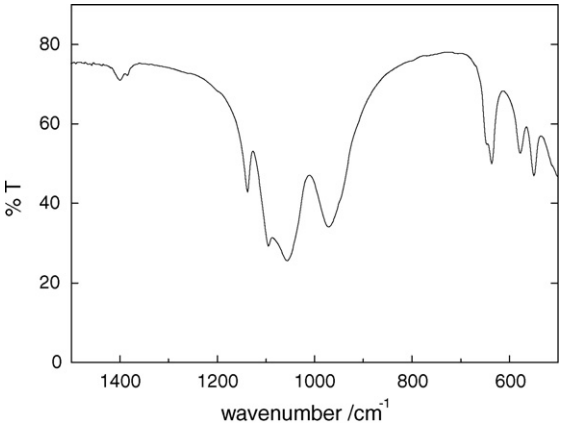

Fig. 4. FT-IR spectrum of MW synthesized $LiFePO_4$.

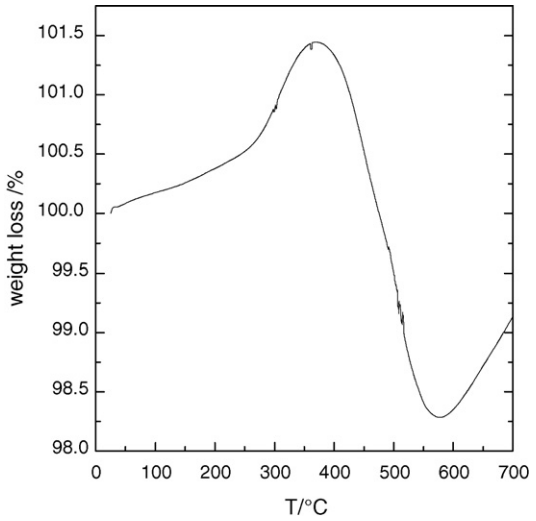

Fig. 5. The TGA curve in O_2 flux of the MW synthesized $LiFePO_4$/C.

Fig. 6 is a SEM image of the MW synthesized $LiFePO_4$/C powder after hand-grinding in a mortar and shows aggregates of small particles with diameters of less than 100 nm. By absorption isotherms of N_2 at 77 K, the BET surface area of the $LiFePO_4$/C was 16 $m^2\,g^{-1}$, a value which compares well with that of materials obtained by sol–gel but is lower than that of materials prepared by solid-state synthesis (44 $m^2\,g^{-1}$) [23].

3.2. Electrochemical tests

Electrodes prepared from $LiFePO_4$/C and carbon-conducting additive ground by ball milling to reduce aggregate size and improve the electric contact among the particles were tested in EC:DMC 2:1 with 1 M $LiPF_6$ by deep galvanostatic charge–discharge cycles at C/10 between 2.8 V and 4.3 V vs. Li to evaluate reversible specific capacity. The delivered charge at the second cycle ranged, at RT, from 80 to 117 mAh g^{-1} of the active material, and increased with temperature, as expected, up to the maximum value of 125 mAh g^{-1} at 45 °C and of 131 mAh g^{-1} at 60 °C. The decrease of the discharge cut-off to 2.2 V increased the delivered charge by ca. 20% at each temperature. Although the values are lower than the theoretical specific capacity, the coulombic efficiency of the cycles was quite high (100%), as shown in Fig. 7, which displays

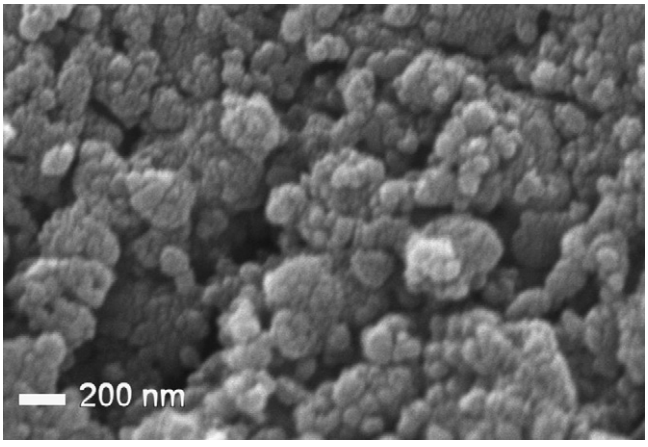

Fig. 6. SEM image of the MW synthesized $LiFePO_4$/C.

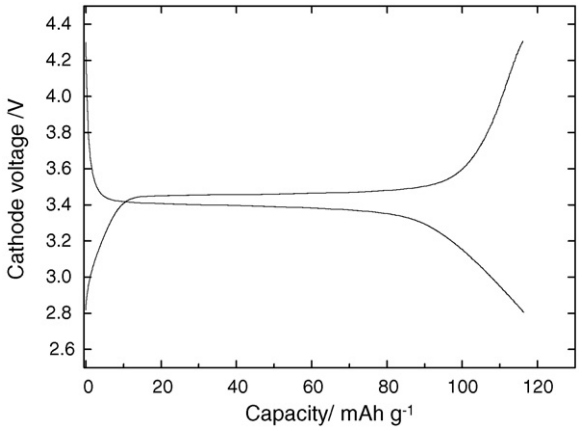

Fig. 7. Second charge–discharge galvanostatic cycle at RT and C/10 of MW $LiFePO_4$/C electrode.

the charge–discharge curves at RT and at 17 mA g^{-1} of the active material of the best performing electrode in terms of specific capacity. The figure also indicates that the two-phase voltage plateau in charge and discharge differ less than 0.1 V. This is important for HEV application since the battery is charged and discharged on board around an intermediate state of charge, i.e. it operates in the so-called 'charge-sustaining' mode. Indeed, the battery provides more than a hundred shallow cycles per day at high C-rate, never approaching the fully charged or discharged state, and low irreversible losses for charge transport in the electrode materials is one of the main goals.

To simulate conditions of battery application in HEV, $LiFePO_4$ electrodes were tested at RT by sequences of galvanostatic pulses of discharge and charge, each of 10 s at 15C, with 300 s rest in open circuit between each pulse; each sequence involved 100 charge and 100 discharge pulses and was carried out after full galvanostatic charge and partial discharge (50% DOD) of the cell at C/10. Table 1 summarizes some results of three sequences performed on an electrode with loading of 0.51 mAh cm^{-2} involving specific current pulses of 2.6 A g^{-1} of active material and shallow charge–discharge corresponding to 4.2% of theoretical capacity. The table shows, for the 10th and 100th pulses of each sequence, the end voltage of the 10 s discharge (V_{ep}), the pulse-specific power related to the active material (P), which was calculated from the delivered energy in the 10 s pulse, and the pulse efficiency (η_p), calculated as the ratio of the experimental energy to that which would be provided if all the charge is delivered at 3.4 V without any irreversible potential loss during the 10 s discharge pulse.

The data in Table 1 show the very good performance of the electrode: the three sequences are similar, in each the potential losses during the discharge pulses even decreased with pulse number and never exceeded 0.6 V, so that the pulse efficiency was quite high.

Table 1
Pulse end voltage, specific power and efficiency of the 10th and 100th charge–discharge 10 s pulses at 15C

Sequence	Pulse number	V_{ep} (V)	P (kW kg^{-1})	η_p (%)
First	10	2.81	7.96	92
	100	3.09	8.22	95
Second	10	2.93	8.18	94
	100	3.05	8.25	95
Third	10	2.93	8.20	94
	100	3.04	8.24	95

Table 2
Specific current, pulse end voltage, specific power and efficiency of the 10th charge–discharge 10 s pulse at different C-rate from 5C to 45C of electrode 1 (0.51 mAh cm^{-2}) and 2 (0.66 mAh cm^{-2})

Electrode	C-rate	Specific current (A g^{-1})	V_{ep} (V)	P (kW kg^{-1})	η_p (%)
1	5	0.8	3.29	2.83	98
	10	1.7	3.21	5.57	96
	15	2.6	3.12	8.23	95
	20	3.4	2.99	10.76	93
	25	4.6	2.85	13.08	90
	30	5.1	2.67	15.28	88
	35	6.0	2.46	17.21	85
	40	6.8	2.20	18.90	82
	45	7.7	1.88	20.20	78
2	5	0.8	3.16	2.75	95
	10	1.7	2.92	5.30	92
	15	2.6	2.69	7.65	88
	20	3.4	2.43	9.77	85
	25	4.6	2.13	11.76	81
	30	5.1	1.77	13.36	77
	35	6.0	1.40	14.45	71
	40	6.8	1.03	15.11	65

This means that when the cell operates at 15C with pulse power of 8 kW kg^{-1} (with respect to the active material), less than 10% of the available energy is lost via irreversible processes.

Since the end voltage of the pulse discharge cannot be lower than 2.2 V according to US DOE standards for HEV battery application, we evaluated the maximum specific power that these electrodes can provide by taking into account this limit as estimated vs. Li for comparison with recently reported data [24]. Sequences of 10 s discharge–charge galvanostatic pulses at RT were performed at different C-rates from 5C to 45C, with 5C increment. Each pulse was followed by 300 s in open circuit, but at each C-rate the sequence involved only 10 charge and 10 discharge pulses and all the sequences from 5C to 45C were carried out after galvanostatic full charge and partial discharge of the cell (50% DOD) at C/10. Table 2 has the results of the 10th pulse at each C-rate performed on two electrodes with different loading, i.e. electrode 1 with 0.51 mAh cm^{-2} and electrode 2 with 0.66 mAh cm^{-2}. The maximum specific power values for electrode 1 and 2 are 18.9 kW kg^{-1} and 11.4 kW kg^{-1} (interpolated value) of active material at current pulses of 6.8 A g^{-1} and 4.1 A g^{-1}, respectively; the 82% pulse efficiency is very high for both electrodes. These results compare well, and even outperform, those recently reported for conventionally prepared $LiFePO_4$ cathode materials [24]. The maximum specific power claimed for the latter, with 84% active material and loading of ca. 1 mAh cm^{-2}, was 3.88 kW kg^{-1} of total electrode mass, including current collector mass of 3.22 mg cm^{-2}, and pulse efficiency ranged from 60% to 70%. The electrodes we prepared had 77% $LiFePO_4$/C and 3.34 mg cm^{-2} current collector. If we take electrode 2, the worst performing, the maximum specific power per total electrode mass is 5.18 kW kg^{-1} and energy losses of 20% instead of 30–40%.

4. Conclusions

Our results confirm the efficacy of MW synthesis for nanometric $LiFePO_4$. However, we were unable to control crystallite size in the range 20–37 nm because of the very short effective synthesis time, which may be related to the fact that, unlike the domestic version, the scientific MW oven operates in single-mode and assures a more homogeneous irradiation of the sample.

Despite the low delivered charge during deep galvanostatic discharge at C/10, the MW $LiFePO_4$/C electrodes tested in EC–DMC 1 M $LiPF_6$ and at RT provided very good results when shallow charge–discharge pulses were performed to simulate operating conditions of batteries for HEV. The maximum specific power and, particularly, the 80% pulse efficiency of these electrodes exceeded the values for conventionally prepared $LiFePO_4$. This makes MW synthesis of $LiFePO_4$/C a very promising route for mass production at low energy costs of this positive electrode material for full-HEV batteries.

Acknowledgements

The authors wish to thank MIUR (Italy) for financial support under the project PRIN 2005 “Nanostructured cathode materials yielded by microwave-assisted synthesis for primary and rechargeable lithium batteries for applications in the biomedical and transportation fields”.

References

[1] A.K. Padhi, K.S. Nanjundaswamy, J.B. Goodenough, J. Electrochem. Soc. 144 (1997) 1188–1194.
[2] M. Anderman, Status and prospects technology for hybrid electric vehicles, including plug-in hybrid vehicles, Briefing to the U.S. Senate Committee on Energy and Natural Resources by the President of Advanced Automotive Batteries, 26 January 2007. http://energy.senate.gov/public/_files/andermantestimony.pdf.
[3] N. Ravet, Y. Chouinard, J.F. Magnan, S. Besner, M. Gauthier, M. Armand, J. Power Sources 97–98 (2001) 503–507.
[4] H. Huang, S.-C. Yin, L.F. Nazar, Electrochem. Solid-State Lett. 4 (2001) A170–A172.
[5] P.P. Prosini, D. Zane, M. Pasquali, Electrochim. Acta 46 (2001) 3517–3523.
[6] F. Croce, A. D'Epifanio, J. Hassoun, A. Deptula, T. Olczac, B. Scrosati, Electrochem. Solid-State Lett. 5 (2002) A47–A50.
[7] C.W. Kim, J.S. Park, K.S. Lee, J. Power Sources 163 (2006) 144–150.
[8] S.-Y. Chung, J.T. Bloking, Y.-M. Chiang, Nat. Mater. 1 (2002) 123–128.
[9] M. Piana, B.L. Cushing, J.B. Goodenough, N. Penazzi, Solid-State Ionics 175 (2004) 233–237.
[10] R. Dominko, M. Bele, M. Gaberscek, M. Remskar, D. Hanzel, J.M. Goupil, S. Pejovnik, J. Jamnik, J. Power Sources 153 (2006) 274–280.
[11] S. Franger, F. Le Cras, C. Bourbon, H. Rouault, J. Power Sources 119–121 (2003) 252–257.
[12] G. Meligrana, C. Geraldi, A. Tuel, S. Bodoardo, N. Penazzi, J. Power Sources 160 (2006) 516–522.
[13] M. Higuchi, K. Katayama, Y. Azuma, M. Yukawa, M. Suhara, J. Power Sources 119–121 (2003) 258–261.
[14] K.S. Park, J.T. Son, H.T. Chung, S.J. Kim, C.H. Lee, H.G. Kim, Electrochem. Commun. 5 (2003) 839–842.
[15] M.-S. Song, Y.-M. Kang, J.-H. Kim, H.-S. Kim, D.-Y. Kim, H.-S. Kwon, J.-Y. Lee, J. Power Sources 166 (2007) 260–265.
[16] L. Wang, Y. Huang, R. Jiang, D. Jia, Electrochim. Acta 52 (2007) 6778–6783.
[17] W. Li, J. Ying, C. Wan, C. Jiang, J. Gao, C. Tang, J. Solid-State Lett. 11 (2007) 799–803.
[18] C. Arbizzani, S. Beninati, L. Damen, M. Mastragostino, Solid-State Ionics 178 (2007) 393–398.
[19] X.-Z. Liao, Z.-F. Ma, L. Wang, X.-M. Zhang, Y. Jiang, Y.-S. He, Electrochem. Solid-State Lett. 7 (2004) A522–A525.
[20] Y. Sundarayya, K.C. Kumara Swamy, C.S. Sunandana, Mater. Res. Bull. 42 (2007) 1942–1948.
[21] S. Yang, Y. Song, P.Y. Zavalij, M.S. Whittingam, Electrochem. Commun. 4 (2002) 239–244.
[22] I. Belharouack, C. Johnson, K. Amine, Electrochem. Commun. 7 (2005) 983–988.
[23] R. Dominko, J.M. Goupil, M. Bele, M. Gaberscek, M. Remskar, D. Hanzel, J. Jamnik, J. Electrochem. Soc. 152 (2005) A858–A863.
[24] I.V. Thorat, V. Mathur, J.N. Harb, D.R. Wheeler, J. Power Sources 162 (2006) 673–678.